Scientific Research and Essays Vol. 6(11), pp. 2286-2295, 4 June, 2011
Available online at http://www.academicjournals.org/SRE
DOI: 10.5897/SRE10.285
ISSN 1992-2248 ©2011 Academic Journals

Full Length Research Paper

A study on the influence of transverse shear and rotary inertia on the dynamic stability of cylindrical shells made from functionally graded material

F. Ebrahimi

Department of Mechanical Engineering, University of Tehran, Tehran, Iran. E-mail: febrahimy@ut.ac.ir.
Tel: +98 21 88005677. Fax: +98 21 88013029.

Accepted 6 May, 2011

In this paper, dynamic stability analysis of functionally graded cylindrical shells subjected to combined static and periodic axial forces is presented, considering the effect of transverse shear and rotary inertia. Material properties of functionally graded cylindrical shells are considered as temperature dependent and graded in the thickness direction according to a power-law distribution in terms of the volume fractions of the constituents. Numerical results for silicon nitride-nickel cylindrical shells are presented based on two different methods of first-order shear deformation theory, considering the transverse shear strains and the rotary inertias and the classical shell theory. The results obtained show that the effect of transverse shear and rotary inertias on dynamic stability of functionally graded cylindrical shells subjected to combined static and periodic axial forces is dependent on the material composition, the temperature environment, the amplitude of static load, the deformation mode, and the shell geometry parameters.

Key words: Functionally graded material, transverse shear, rotary inertia, dynamic stability, cylindrical shell.

INTRODUCTION

Functionally graded materials (FGMs) are being increasingly considered in various applications to maximize strengths and integrities of many engineering structures. FGMs have received considerable attention in many engineering applications, since they were first reported in 1984 in Japan (Koizumi and Niino, 1995). FGMs are composite materials, microscopically inhomogeneous, in which the mechanical properties vary smoothly and continuously from one surface to the other. This is achieved by gradually varying the volume fraction of the constituent materials. FGMs were initially designed as thermal barrier materials for aerospace structures and fusion reactors and now they are also considered as potential structural materials for future high-speed spacecrafts. Formulation and theoretical analysis of the FGM plates and shells were presented by Reddy (2004), Reddy and Chin (1998), Arciniega and Reddy (2007) and Praveen et al. (1999). Shell structure made up of this composite material (FGM) is also one of the basic structural elements used in many engineering structures.

Despite the evident importance in practical applications, investigations on the static and dynamic characteristics of FGM shell structures are still limited in number. Among those available, Loy et al. (1999) investigated the free vibration of simply supported FGM cylindrical shells, which was later extended by Pradhan et al. (2000) to cylindrical shells under various end supporting conditions. Gong et al. (1999) presented elastic response analysis of simply supported FGM cylindrical shells under low-velocity impact. Ng et al. (2001) studied dynamic instability of simply supported FGM cylindrical shells, a normal-mode expansion and Bolotin method were used to determine the boundaries of the unstable regions. In all the aforementioned studies, theoretical formulations were all based on classical shell theory, that is neglecting the effect of transverse shear strains. Using Love's shell theory and the Galerkin method, Sofiyev (2005) presented an analytic solution for the stability behavior of cylindrical shells made of compositionally (or functionally) graded ceramic–metal materials under the axial compressive loads.

This paper studies the effect of transverse shear and

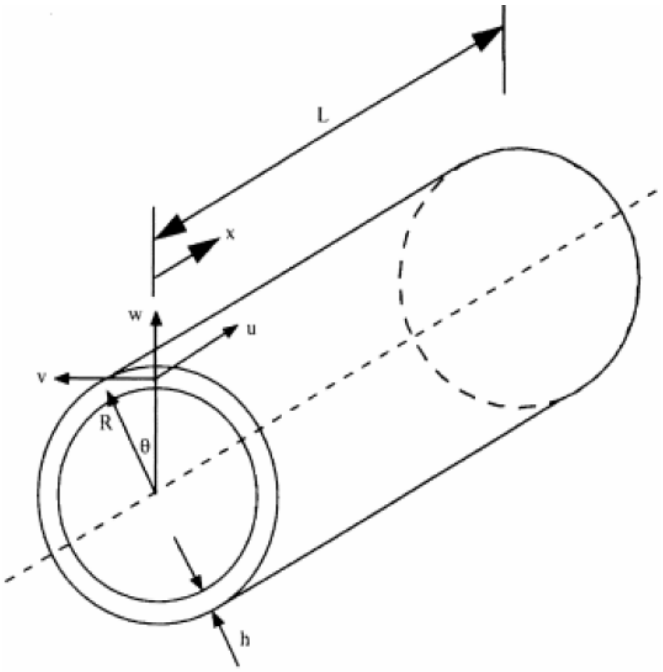

Figure 1. Coordinate system of the FGM cylindrical shell.

rotary inertias on dynamic stability of the functionally graded (FG) cylindrical shells subjected to combined static and periodic axial forces, through a comparison of results obtained by using two different methods such as the first-order shear deformation theory (FSDT) considering the transverse shear strains and the rotary inertias and the classical shell theory (CST). Material properties of FG cylindrical shells are considered as temperature dependent and graded in the thickness direction, according to a power-law distribution in terms of the volume fractions of the constituents. The results obtained show that the effect of transverse shear and rotary inertias on dynamic stability of FG cylindrical shells subjected to combined static and periodic axial forces is dependent on the material composition, the temperature environment, the amplitude of static load, the deformation mode, and the shell geometry parameters. It was found that the effect of transverse shear and rotary inertias on dynamic stability of FG cylindrical shells subjected to combined static and periodic axial forces is not neglected in some cases. The new features of the effect of transverse shear and rotary inertias on dynamic stability of FG cylindrical shells and some meaningful results in this paper, are helpful for the application and the design of nuclear reactors, space planes and chemical plants, in which FG cylindrical shells act as basic elements.

THEORY AND FORMULATIONS

An FGM cylindrical shell with mean radius of *R,* thickness *h,* and the length *L* is shown in Figure 1. The displacement components in the *x,* θ and *z* direction are denoted by *u, v* and *w* respectively. The pulsating axial load is given by

$$N_a = N_o + N_d \cos Pt \tag{1}$$

Where *P* is the frequency of excitation in radians per unit time.

The material properties of FGM cylindrical shells with both temperature dependent and position dependent are accurately modeled, by using a simple rule of mixtures for the stiffness parameters coupled with the temperature dependent properties of the constituents. The volume fraction is described by a spatial function as follows

$$V(z) = (z/h + 1/2)^{\Phi} \quad , \quad (0 \le \Phi \le \infty), \tag{2}$$

where Φ expresses the volume fraction exponent.

The combination of these functions gives rise to the effective properties of FGMs. An FGM cylindrical shell that is metal rich at the inner surface and ceramic rich at the outer surface is defined as Type A. The corresponding effective material properties are expressed as

$$F_{eff}(T,z) = F_c(T)V(z) + F_m(T)(1 - V(z)) \tag{3}$$

Where F_{eff} is the effective material property of the FGM cylindrical shell, including the effective elastic modulus, effective mass density and effective Poisson's ratio. F_c and F_m are the temperature dependent properties of the ceramic and metal, respectively.

On the other hand, an FGM cylindrical shell that is ceramic rich at the inner surface and metal rich at the outer surface is defined as Type B, whose effective material properties are given by

$$F_{eff}(T,z) = F_m(T)V(z) + F_c(T)(1 - V(z)) \tag{4}$$

Based on FSDT, the equations of motion for an FGM cylindrical shell under axially dynamic load according to Sofiyev (2005) are as follows

$$\frac{\partial N_1}{\partial x} + \frac{1}{R}\frac{\partial N_6}{\partial \theta} = I_1 u'' + I_2 \phi_1'' \tag{5}$$

$$\frac{\partial N_6}{\partial x} + \frac{1}{R}\frac{\partial N_1}{\partial \theta} + \frac{1}{R}Q_2 + N_a \frac{\partial^2 v}{\partial x^2} = I_1 v'' + I_2 \phi_2'' \tag{6}$$

$$\frac{\partial Q_1}{\partial x}+\frac{1}{R}\frac{\partial Q_2}{\partial \theta}-\frac{N_2}{R}+N_a\frac{\partial^2 w}{\partial x^2}=I_1 w'' \tag{7}$$

$$\frac{\partial M_1}{\partial x}+\frac{1}{R}\frac{\partial M_6}{\partial \theta}-Q_1=I_2 u''+I_3\phi_1'' \tag{8}$$

$$\frac{\partial M_6}{\partial x}+\frac{1}{R}\frac{\partial M_2}{\partial \theta}-Q_2=I_2 v''+I_3\phi_2'' \tag{9}$$

where ϕ_1 and ϕ_2 are the rotations of a normal to the reference surface, $I_i(i=1,2,3)$ is the mass inertia terms defined as

$$(I_1,I_2,I_3)=\int_{-\frac{h}{2}}^{\frac{h}{2}}\rho(z)(1,z,z^2)dz \tag{10}$$

and $\rho(z)$ is the effective mass density of FGMs. The stress resultants of FGM cylindrical shells are given by

$$\begin{pmatrix}N_1\\N_2\\N_6\\M_1\\M_2\\M_6\end{pmatrix}=\begin{pmatrix}A_{11}&A_{12}&0&B_{11}&B_{12}&0\\A_{21}&A_{22}&0&B_{21}&B_{22}&0\\0&0&A_{66}&0&0&B_{66}\\B_{11}&B_{12}&0&D_{11}&D_{12}&0\\B_{21}&B_{22}&0&D_{21}&D_{22}&0\\0&0&B_{66}&0&0&D_{66}\end{pmatrix}\begin{pmatrix}\varepsilon_1\\\varepsilon_2\\\varepsilon_6\\\kappa_1\\\kappa_2\\\kappa_6\end{pmatrix}$$

$$\begin{pmatrix}Q_1\\Q_2\end{pmatrix}==\begin{pmatrix}C_{44}&0\\0&C_{55}\end{pmatrix}\begin{pmatrix}\varepsilon_5\\\varepsilon_4\end{pmatrix} \tag{11}$$

where A_{ij} , B_{ij} , D_{ij} and C_{ij} are ,respectively, the extensional, coupling, bending, and shear stiffness, which are given by

$$(A_{ij},B_{ij},D_{ij})=\int_{-\frac{h}{2}}^{\frac{h}{2}}Q_{ij}(1,z,z^2)dz,\quad (i=1,2,6)$$

$$Q_{11}=Q_{22}=\frac{E_{eff}}{1-\nu_{eff}^{\ 2}}\quad Q_{12}=Q_{21}=\frac{\nu_{eff}E_{eff}}{A(1-\nu_{eff}^{\ 2})}\quad C_{44}=\int_{-\frac{h}{2}}^{\frac{h}{2}}Q_{44}dz\quad Q_{66}=\frac{E_{eff}}{2A(1+\nu_{eff})}$$

$$Q_{44}=\kappa\frac{E_{eff}}{2(1+\nu_{eff})}\quad Q_{55}=Q_{44}/A\quad C_{55}=\int_{-\frac{h}{2}}^{\frac{h}{2}}Q_{55}dz\quad A=1+z/R \tag{12}$$

where E_{eff} and $\nu_{eff.}$ are the effective elastic modulus and effective Poisson's ratio of FGM cylindrical shells, respectively. κ is the shear correction factor introduced by Reddy (2004) and is equal to 5/6 . The strains are expressed as

$$\varepsilon_1=\frac{\partial u}{\partial x}\quad,\quad \varepsilon_2=\frac{1}{R}\left(\frac{\partial v}{\partial \theta}+w\right)\quad,\quad \varepsilon_6=\frac{\partial v}{\partial x}+\frac{1}{R}\frac{\partial u}{\partial \theta}\quad,$$

$$\varepsilon_4=\phi_2+\frac{1}{R}\frac{\partial w}{\partial \theta}\quad,\quad \varepsilon_5=\phi_1+\frac{\partial w}{\partial x}\quad,\quad \kappa_1=\frac{\partial \phi_1}{\partial x}\quad,$$

$$\kappa_2=\frac{1}{R}\frac{\partial \phi_2}{\partial \theta}\ ,\ \kappa_6=\frac{\partial \phi_2}{\partial x}+\frac{1}{R}\frac{\partial \phi_1}{\partial \theta} \tag{13}$$

Utilizing Equations (5) to (9), (11) and (13), the equations of motion can be expressed in terms of generalized displacement (u,v,w,ϕ_1,ϕ_2) as follows

$$L_1(u,v,w,\phi_1,\phi_2)=I_1u''+I_2\phi_1'' \tag{14}$$

$$L_2(u,v,w,\phi_1,\phi_2)+N_a\frac{\partial^2 v}{\partial x^2}=I_1v''+I_2\phi_2'' \tag{15}$$

$$L_3(u,v,w,\phi_1,\phi_2)+N_a\frac{\partial^2 w}{\partial x^2}=I_1w'' \tag{16}$$

$$L_4(u,v,w,\phi_1,\phi_2)=I_2u''+I_3\phi_1'' \tag{17}$$

$$L_5(u,v,w,\phi_1,\phi_2)=I_2v''+I_3\phi_2'' \tag{18}$$

By neglecting terms I_2 and I_3 involved in Equations (5) to (9) and setting

$$\phi_1=-\frac{\partial w}{\partial x},\ \ \phi_2=-\frac{1}{R}\frac{\partial w}{\partial \theta}, \tag{19}$$

The equations of motion based on a classical shell theory can be easily obtained. Here, the two ends of FGM cylindrical shells are considered as simply supported, so that a solution for the motion Equations (14) to (18) can be described by

$$u_{mn}=\overline{A}_{mn}e^{i\omega t}\cos\lambda_m\ x\cos n\theta$$

$$v_{mn}=\overline{B}_{mn}e^{i\omega t}\sin\lambda_m\ x\sin n\theta$$

$$w_{mn}=\overline{C}_{mn}e^{i\omega t}\sin\lambda_m\ x\cos n\theta$$

$$\phi_{1mn}=\overline{H}_{mn}e^{i\omega t}\cos\lambda_m\ x\cos n\theta$$

$$\phi_{2mn}=\overline{K}_{mn}e^{i\omega t}\sin\lambda_m\ x\sin n\theta \tag{20}$$

where $\lambda_m = \frac{m\pi}{L}$., n represents the number of circumferential waves and m represents he number of axial half-waves.

Substituting Equation (20) into Equations (14) to (18) and letting $N_d = 0$ in Equation (1), yields

$$\left(\begin{bmatrix} T_{11} & T_{12} & T_{13} & T_{14} & T_{15} \\ T_{21} & T_{12}+\lambda_m^2 N_0 & T_{23} & T_{24} & T_{25} \\ T_{31} & T_{31} & T_{33}+\lambda_m^2 N_0 & T_{34} & T_{35} \\ T_{41} & T_{42} & T_{43} & T_{44} & T_{45} \\ T_{51} & T_{52} & T_{53} & T_{54} & T_{55} \end{bmatrix} - \omega^2 \begin{bmatrix} I_1 & 0 & 0 & I_2 & 0 \\ 0 & I_1 & 0 & 0 & I_2 \\ 0 & 0 & I_1 & 0 & 0 \\ I_2 & 0 & 0 & I_3 & 0 \\ 0 & I_2 & 0 & 0 & I_3 \end{bmatrix}\right)\begin{Bmatrix} \overline{A}_{mn} \\ \overline{B}_{mn} \\ \overline{C}_{mn} \\ \overline{H}_{mn} \\ \overline{K}_{mn} \end{Bmatrix} = \begin{Bmatrix} 0 \\ 0 \\ 0 \\ 0 \\ 0 \end{Bmatrix} \quad (21)$$

where T_{ij} is given in Appendix A.

To solve the equations of motion containing the dynamic load N_d, a solution is sought in the form shown as follows

$$u = \sum_{j=1}^{5}\sum_{m=1}^{\infty}\sum_{n=1}^{\infty} q_{mnj}(t)U_{mnj}(x,\theta) = \sum_{j=1}^{5}\sum_{m=1}^{\infty}\sum_{n=1}^{\infty} q_{mnj}(t)\overline{A}_{mnj}\cos\lambda_m x\cos n\theta \quad (22)$$

$$v = \sum_{j=1}^{5}\sum_{m=1}^{\infty}\sum_{n=1}^{\infty} q_{mnj}(t)V_{mnj}(x,\theta) = \sum_{j=1}^{5}\sum_{m=1}^{\infty}\sum_{n=1}^{\infty} q_{mnj}(t)\overline{B}_{mnj}\sin\lambda_m x\sin n\theta \quad (23)$$

$$w = \sum_{j=1}^{5}\sum_{m=1}^{\infty}\sum_{n=1}^{\infty} q_{mnj}(t)W_{mnj}(x,\theta) = \sum_{j=1}^{5}\sum_{m=1}^{\infty}\sum_{n=1}^{\infty} q_{mnj}(t)\overline{C}_{mnj}\sin\lambda_m x\cos n\theta \quad (24)$$

$$\phi_1 = \sum_{j=1}^{5}\sum_{m=1}^{\infty}\sum_{n=1}^{\infty} q_{mnj}(t)\theta_{xmnj}(x,\theta) = \sum_{j=1}^{5}\sum_{m=1}^{\infty}\sum_{n=1}^{\infty} q_{mnj}(t)\overline{H}_{mnj}\cos\lambda_m x\cos n\theta \quad (25)$$

$$\phi_2 = \sum_{j=1}^{5}\sum_{m=1}^{\infty}\sum_{n=1}^{\infty} q_{mnj}(t)\theta_{\theta mnj}(x,\theta) = \sum_{j=1}^{5}\sum_{m=1}^{\infty}\sum_{n=1}^{\infty} q_{mnj}(t)\overline{K}_{mnj}\sin\lambda_m x\sin n\theta \quad (26)$$

where $q_{mnj}(t)$ is a generalized co-ordinate, and U_{mnj}, V_{mnj}, W_{mnj}, θ_{xmnj} and $\theta_{\theta mnj}$ are the modal function of FGM cylindrical shells with simply supported ends, under the axially static load N_0. Substituting Equations (22) to (26) into Equations (14) to (18), yields

$$L_1(U_{mnj},V_{mnj},W_{mnj},\theta_{xmnj},\theta_{\theta mnj}) = -I_1\omega_{mnj}^2 U_{mnj} - I_2\omega_{mnj}^2 H_{mnj} \quad (27)$$

$$L_2(U_{mnj},V_{mnj},W_{mnj},\theta_{xmnj},\theta_{\theta mnj}) - N_0\lambda_m^2 V_{mnj} = -I_1\omega_{mnj}^2 V_{mnj} - I_2\omega_{mnj}^2\theta_{\theta mnj} \quad (28)$$

$$L_3(U_{mnj},V_{mnj},W_{mnj},\theta_{xmnj},\theta_{\theta mnj}) - N_0\lambda_m^2 W_{mnj} = -I_1\omega_{mnj}^2 W_{mnj} \quad (29)$$

$$L_4(U_{mnj},V_{mnj},W_{mnj},\theta_{xmnj},\theta_{\theta mnj}) = -I_2\omega_{mnj}^2 U_{mnj} - I_3\theta_{xmnj} \quad (30)$$

$$L_5(U_{mnj},V_{mnj},W_{mnj},\theta_{xmnj},\theta_{\theta mnj}) = -I_2\omega_{mnj}^2 V_{mnj} - I_3\theta_{\theta mnj} \quad (31)$$

Equations (14) to (18) may be rewritten as

$$\sum_{j=1}^{5}\sum_{m=1}^{\infty}\sum_{n=1}^{\infty}\left(q''_{mnj} + \omega_{mnj}^2 q_{mnj}\right)\left(I_1 A_{mnj} + I_2 H_{mnj}\right)\cos\lambda_m x\cos n\theta = 0 \quad (32)$$

$$\sum_{j=1}^{5}\sum_{m=1}^{\infty}\sum_{n=1}^{\infty}\left(q''_{mnj} + \omega_{mnj}^2 q_{mnj}\right)\left(I_1 B_{mnj} + I_2 K_{mnj}\right)\sin\lambda_m x\sin n\theta + N_d\cos Pt\sum_{j=1}^{5}\sum_{m=1}^{\infty}\sum_{n=1}^{\infty}\lambda_m^2 B_{mnj}q_{mnj}\sin\lambda_m x\sin n\theta = 0 \quad (33)$$

$$\sum_{j=1}^{5}\sum_{m=1}^{\infty}\sum_{n=1}^{\infty}\left(q''_{mnj} + \omega_{mnj}^2 q_{mnj}\right)I_1 C_{mnj}\sin\lambda_m x\cos n\theta + N_d\cos Pt\sum_{j=1}^{5}\sum_{m=1}^{\infty}\sum_{n=1}^{\infty}\lambda_m^2 C_{mnj}q_{mnj}\sin\lambda_m x\cos n\theta = 0 \quad (34)$$

$$\sum_{j=1}^{5}\sum_{m=1}^{\infty}\sum_{n=1}^{\infty}\left(q''_{mnj} + \omega_{mnj}^2 q_{mnj}\right)\left(I_2 A_{mnj} + I_3 H_{mnj}\right)\cos\lambda_m x\cos n\theta = 0 \quad (35)$$

$$\sum_{j=1}^{5}\sum_{m=1}^{\infty}\sum_{n=1}^{\infty}\left(q''_{mnj} + \omega_{mnj}^2 q_{mnj}\right)\left(I_2 B_{mnj} + I_3 K_{mnj}\right)\sin\lambda_m x\sin n\theta = 0 \quad (36)$$

Making use of the orthogonality condition, Equations (32) to (36) are simplified to

$$\begin{bmatrix} m_1 & 0 & 0 & 0 \\ 0 & m_1 & 0 & 0 \\ 0 & 0 & O & 0 \\ 0 & 0 & 0 & m_{5N^2} \end{bmatrix}\begin{Bmatrix} q''_1 \\ q''_2 \\ M \\ q''_{5N^2} \end{Bmatrix} + \left(\begin{bmatrix} k_1 & 0 & 0 & 0 \\ 0 & k_2 & 0 & 0 \\ 0 & 0 & O & 0 \\ 0 & 0 & 0 & k_{5N^2} \end{bmatrix} - N_d\cos Pt\begin{bmatrix} \overline{Q}_1 & 0 & 0 & 0 \\ 0 & \overline{Q}_2 & 0 & 0 \\ 0 & 0 & O & 0 \\ 0 & 0 & 0 & \overline{Q}_{5N^2} \end{bmatrix}\right)\begin{Bmatrix} q_1 \\ q_2 \\ M \\ q_{5N^2} \end{Bmatrix} = 0 \quad (37)$$

where

$$m_I=\frac{\pi l}{2}\left[\left(I_1\overline{B}_I+I_2\overline{K}_I\right)^2+\left(I_1\overline{A}_I+I_2\overline{H}_I\right)^2+\left(I_1\overline{C}_I\right)^2+\left(I_2\overline{A}_I+I_3\overline{H}_I\right)^2+\left(I_2\overline{B}_I+I_3\overline{K}_I\right)^2\right]$$

$$k_I=\omega_I^2 m_I,\quad \overline{Q}_I=-\frac{\pi L}{2}\lambda_m^2\left[\overline{B}_I\left(I_1\overline{B}_I+I_2\overline{K}_I\right)+I_1\overline{C}_I{}^2\right] \tag{38}$$

$$(m,n)=(1,1):\quad I=1(j=1),\ 2(j=2),\quad 3(j=3),\quad 4(j=4),\quad 5(j=5);$$
$$(m,n)=(1,2):\quad I=6(j=1),\ 7(j=2),\quad 8(j=3),\quad 9(j=4),\quad 10(j=5);$$

$$(m,n)=(1,N):\quad I=5(N-4)\,(j=1),\ 5(N-3)\,(j=2),\quad 5N\,(j=5);$$
$$(m,n)=(2,1):\quad I=5N+1\,(j=1),\ 5N+2\,(j=2),\quad 5N+5\,(j=5);$$

$$(m,n)=(N,N):\quad I=5N^2-4\,(j=1),\ 5N^2-3\,(j=2),\quad 5N^2\,(j=5); \tag{39}$$

In the aforestated formula, the coefficients of mode shapes $\overline{A}_I$, $\overline{B}_I$, $\overline{C}_I$, $\overline{H}_I$ and $\overline{K}_I$ can be obtained from Equation (21). Based on the classical shell theory and the orthogonality condition, Equation (37) can be simplified to

$$\begin{bmatrix} m_1 & 0 & 0 & 0\\ 0 & m_1 & 0 & 0\\ 0 & 0 & \mathrm{O} & 0\\ 0 & 0 & 0 & m_{3N^2}\end{bmatrix}\begin{Bmatrix} q_1''\\ q_2''\\ M\\ q_{3N^2}''\end{Bmatrix}+$$
$$\left(\begin{bmatrix} k_1 & 0 & 0 & 0\\ 0 & k_2 & 0 & 0\\ 0 & 0 & \mathrm{O} & 0\\ 0 & 0 & 0 & k_{3N^2}\end{bmatrix}-N_d\cos Pt\begin{bmatrix} \overline{Q}_1 & 0 & 0 & 0\\ 0 & \overline{Q}_2 & 0 & 0\\ 0 & 0 & \mathrm{O} & 0\\ 0 & 0 & 0 & \overline{Q}_{3N^2}\end{bmatrix}\right)\begin{Bmatrix} q_1\\ q_2\\ M\\ q_{3N^2}\end{Bmatrix}=\begin{Bmatrix} 0\\ 0\\ M\\ 0\end{Bmatrix} \tag{40}$$

where

$$m_I=\frac{\pi l}{2}\left[\left(I_1\overline{B}_I\right)^2+\left(I_1\overline{A}_I\right)^2+\left(I_1\overline{C}_I\right)^2\right],\qquad k_I=\omega_I^2 m_I,$$
$$\overline{Q}_I=-\frac{\pi L}{2}\lambda_m^2\left[\overline{B}_I\left(I_1\overline{B}_I\right)+I_1\overline{C}_I{}^2\right],\quad I=1,2,3,...,3N^2 \tag{41}$$

The coefficients $\overline{A}_I$, $\overline{B}_I$, $\overline{C}_I$ in Equations (40) can be obtained from Equation (24). Equations (37) and (40) are in the form of a second order differential equation with periodic coefficients of the Mathieu-Hill type. Using the method presented by Bolotin (1964), the regions of unstable solutions are separated by periodic solutions. As a first approximation, the periodic solutions with period 2*T* can be sought in the form

$$q_I=a_I\sin\frac{Pt}{2}+b_I\cos\frac{Pt}{2} \tag{42}$$

where a_I and b_I are arbitrary constants. Substituting Equation (42) into Equations (37) and (40), and equating the coefficients of the $\sin Pt/2$ and $\cos Pt/2$ terms, a set of linear homogeneous algebraic equations in terms of a_I and b_I can be obtained. The conditions for non-trivial solutions for the linear homogeneous algebraic equations are

$$-\frac{1}{4}\overline{P}_I^2 m_I+k_I-\frac{1}{2}N_d\overline{Q}_I=0 \tag{43}$$

$$-\frac{1}{4}\overline{P}_I^2 m_I+k_I+\frac{1}{2}N_d\overline{Q}_I=0 \tag{44}$$

Each unstable region is bounded by two lines which originate from a common point from the *P*-axis. The branches emanate at $N_d=0$ from the $2\omega_I$. The left and right branch correspond with $\overline{P}_I=\sqrt{\frac{4k_I+2N_d\overline{Q}_I}{m_I}}$ *and* $\overline{P}_I=\sqrt{\frac{4k_I-2N_d\overline{Q}_I}{m_I}}$ $(N_d>0)$ or $\overline{P}_I=\sqrt{\frac{4k_I-2N_d\overline{Q}_I}{m_I}}$ *and* $\overline{P}_I=\sqrt{\frac{4k_I+2N_d\overline{Q}_I}{m_I}}$ $(N_d<0)$.

RESULTS AND DISCUSSION

The ceramic material used in this study is silicon nitride and the metal material used is nickel. The density of silicon nitride is ρ_c =2370 kg/m^3 that of nickel is ρ_e =8900 kg/m^3, the Poisson's ratio is ν_c =0.24. for silicon nitride and ν_e =0.31 for nickel, which are independent of the temperature. The elastic moduli are given by Ng et al. (2001).

$$E_c=34843\times10^9\left(1-3.070\times10^{-4}T+2.160\times10^{-7}T^2-8.946\times10^{-11}T^3\right)$$

$$E_m=223.95\times10^9\left(1-2.794\times10^{-4}T-3.998\times10^{-9}T^2\right)$$

where E_c and E_m are the elastic modulus of silicon nitride and nickel, respectively, and *T* is the temperature in Kelvin. Also a computer program has been written in MATLAB software in order to compute the numerical results. Based on the classical shell theory, the points of origin, $P_1=2\times\omega_1\times\alpha$ [the nondimensionalized coefficient $\alpha=2\pi R\times\sqrt{I_1/A_{11}}$, $I=1$, as in (39)] is presented in Table 1, for a silicon nitride-nickel FGM cylindrical shell with simply supported ends, under axial extensional loading, Where the computation parameters are taken as

$$m=n=1,\ N_0=0.5N_{cr},\quad L/R=1,\quad R/h=100.$$

Table 1. Comparison of the points of origin P_1 for a simply supported silicon nitride-nickel FGM cylindrical shell under axial extensional loading.

Φ	P_1 (Type A)		P_1 (Type B)	
	Present	Ng et al. (2001)	Present	Ng et al. (2001)
0	10.955	10.956	10.778	10.774
0.5	10.896	10.894	10.849	10.849
1.0	1.0867	10.865	10.883	10.883
5.0	10.809	10.805	10.936	10.937
10	10.795	10.791	10.945	10.946
∞	10.778	10.773	10.955	10.946

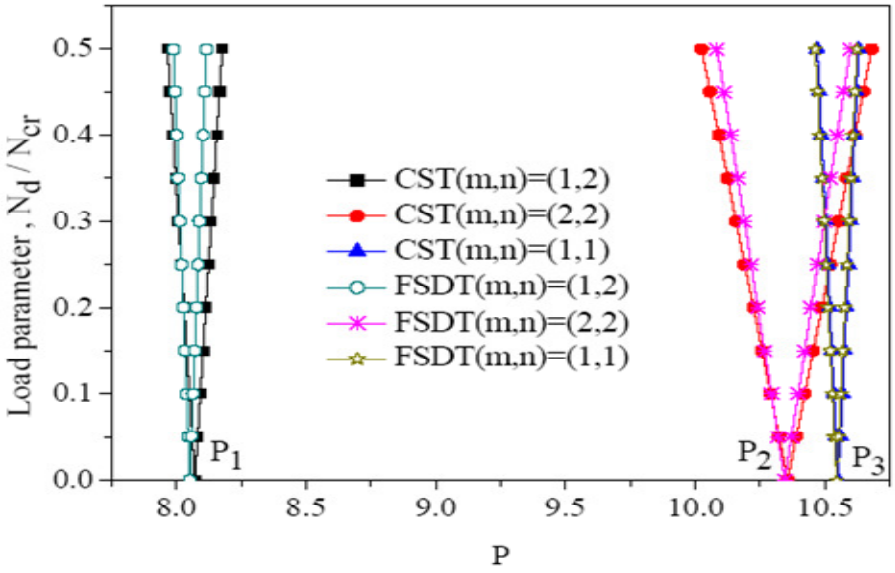

Figure 2. Comparison of CST and FSDT unstable regions for a simply supported silicon nitride-nickel FGM Type A cylindrical shell under combined static axial compressive loading and periodic axial loading (m=1,2 , n=1,2 , $N_0 = 0.5N_{cr}$, L/R=1.0 , T=300K, Φ=1.0, h/R=0.01).

The results in Table 1 present the transverse modes corresponding to the points of origin P_1 , which is a good agreement with Ng et al. (2001). The dynamic instability regions for the first order parametric resonances of a silicon nitride-nickel FGM (Type A) cylindrical shell with simply supported ends, under combined static and periodic axial loads are presented in Figure 2 using the CLT and the FSDT. The effect of the FSDT on the dynamic instability regions is relational to the points of origin, $P_1 = 2\times\omega_6\times\alpha\,(I=6)$, $P_2 = 2\times\omega_{16}\times\alpha\,(I=16)$, $P_3 = 2\times\omega_1\times\alpha\,(I=1)$ [Equation (39), FSDT].

For the points P_1 and P_2 , the dynamic instability regions obtained from the FSDT are less than those obtained from the CST no considering shear deformation and rotary inertias. For the points P_3, the dynamic instability regions are very close for the CST and the FSDT. Where ω_6 , ω_{16} and ω_1 denote the three lowest natural frequency using the FSDT. Figure 3 shows the effect of thickness to radius ratio (h/R) on the first unstable region (corresponding to the point of origin P_1) for a silicon nitride-nickel FGM (Type A) cylindrical shell under combined static axial extensional loading and periodic axial load, based on the FSDT. It is observed that the points of origin of the unstable region are lower for the thinner shells. The angle φ gives a good measure of the size of the unstable region in Figure 3. Here, the unstable regions increase with the increasing thicknesses.

The effect of static axial compressive loading N_o/N_{cr} on unstable angles φ. can be seen from the

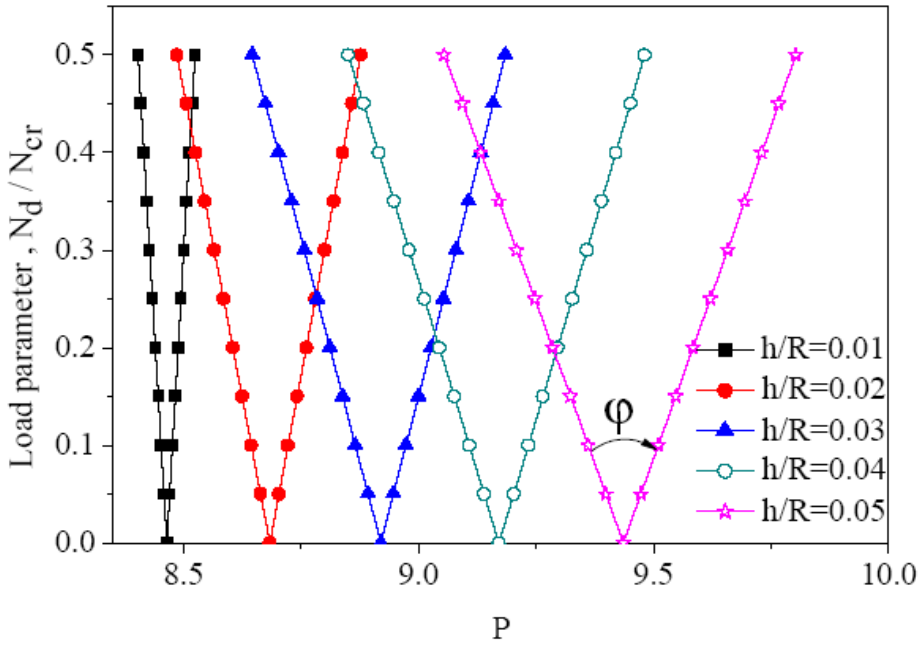

Figure 3. Effect of thickness to radius ratio *h/R* on the first unstable region (corresponding to the points of origin 1 P_1) for a simply supported silicon nitride-nickel FGM Type A cylindrical shell under combined static axial extensional loading and periodic axial load (m=1,2 , n=1,2 , $N_0 = 0.5N_{cr}$, L/R = 1.0 , T = 300K, Φ = 1.0).

results presented in Figure 4, using the CST and the FSDT. The points of origin are, respectively, $P_1 = 2\times\omega_6\times\alpha\ (I=6)$, $P_2 = 2\times\omega_{16}\times\alpha\ (I=16)$, $P_3 = 2\times\omega_1\times\alpha\ (I=1)$, $P_4 = 2\times\omega_{11}\times\alpha\ (I=11)$ [Equation (39), FSDT]. The first four unstable angles φ (corresponding to the points of origin P_1 , P_2 , P_3 , P_4) for a silicon nitride-nickel FGM (Type A) cylindrical shell under combined static axial compressive loading and periodic axial loading are described in Figures 4(a) and (b), respectively.

The unstable region increases as the static axial load increases, and the effect of shear deformation and rotary inertias on the unstable region is dependent on the points of origin. It is shown from the results presented in Figures 4(a) and (b), that the unstable angle for the points P_1 , P_2 and P_4 obtained using the FSDT are less than those obtained using the CST, and when the static axial compressive loading N_o/N_{cr} is larger than 0.4, the third unstable angle (corresponding to the point of origin P_3 and m=1, n=1) is almost the same using the CST and the FSDT. Figures 5(a) to (c) show the effect of volume fraction exponent on the unstable angle φ of a silicon nitride-nickel FGM (Type A) cylindrical shell under combined static axial compressive loading and periodic axial loading, based on two different theories such as the CST and the FSDT. The first three unstable regions (corresponding to the points of origin P_1 , P_2 and P_3) are described in Figures 5(a) to (c), respectively. It is observed that the unstable angle φ nonlinearly increases as the volume fraction exponent Φ increases, the effect of shear deformation and rotary inertias on the unstable angles (corresponding to m=1, n=1) is not only dependent on the points of origin, but also dependent on the volume fraction exponent Φ , the unstable angles for the point P_2 obtained by using the CST and the FSDT are the same.

CONCLUSIONS

This paper reports the result of an investigation into the effect of the FSDT considering rotary inertia and the transverse shear strains on the dynamic instability of FG cylindrical shells with simply-supported ends, under combined static and periodic axial forces. The result obtained using the FSDT is compared with that obtained using CST. The differences between the results from FSDT and the results from CST increase as the deformation mode and thickness increase. It is proved that the unstable angle is different using the CST and the FSDT for the higher mode. It was found that reasonable control can be achieved on the dynamic instability regions by correctly varying the ratio of length to radius,

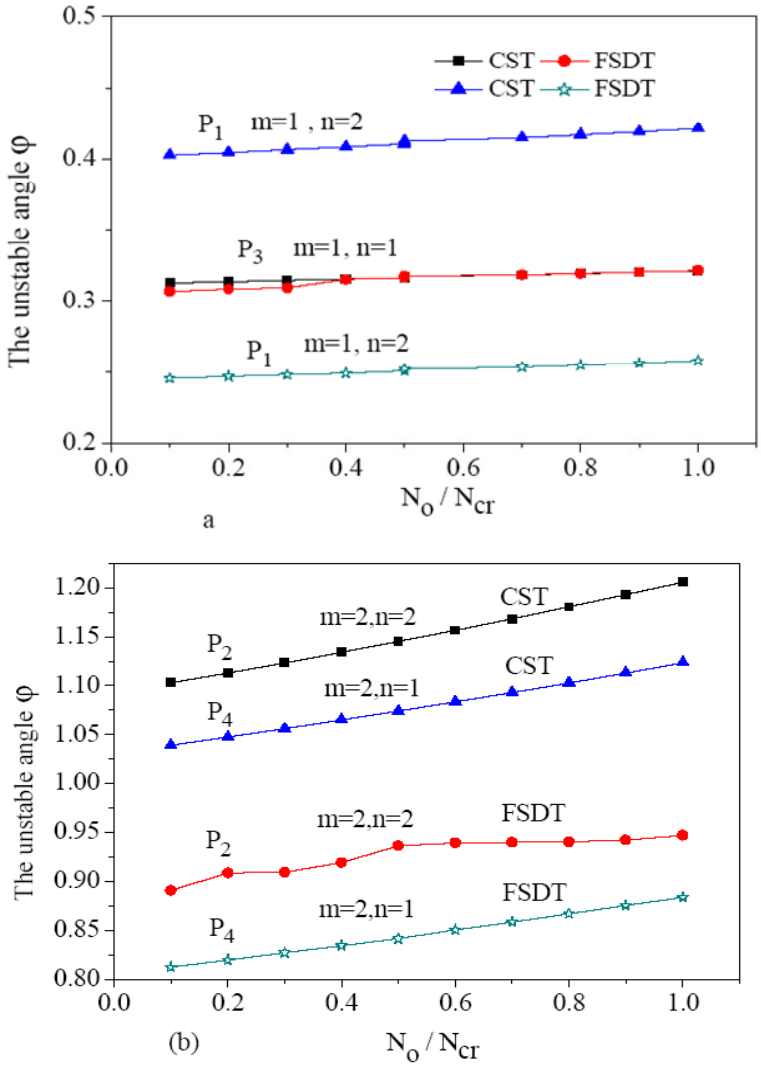

Figure 4. Unstable region φ versus axial compressive loading N_0/N_{cr} for a simply supported silicon nitride-nickel FGM Type A cylindrical shell under combined static axial compressive loading and periodic axial loading (m=1, 2, n=1,2 , L/R=1.0 , T=300K, Φ =1.0, h/R=0.01).

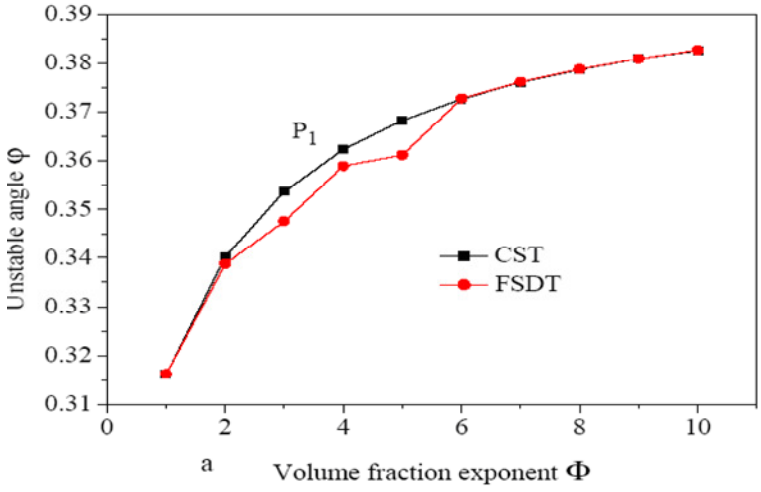

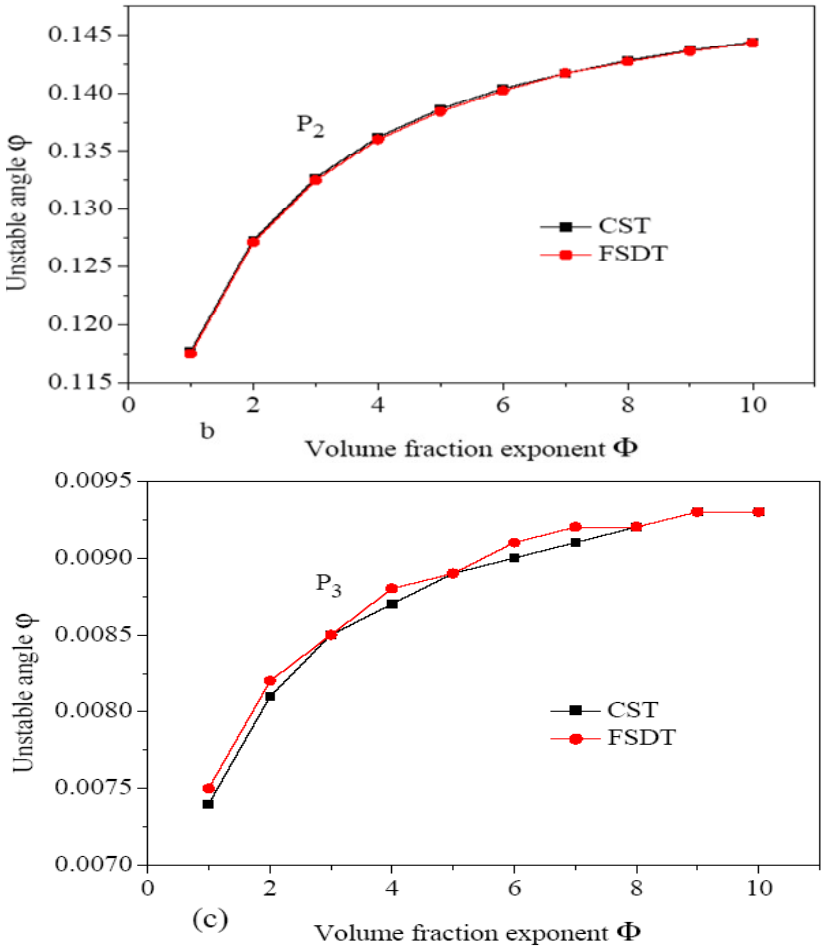

Figure 5. Effect of the volume fraction exponent Φon the unstable angles $\varphi$for a simply supported silicon nitride-nickel FGM Type A cylindrical shell under combined static axial compressive loading and periodic axial loading (m=1, n=1, $N_0 = 0.5N_{cr}$, L/R=1.0 , T=300K, Φ=1.0, h/R=0.01).

the ratio of thickness to radius, the amplitude of static axial load, thermal environment and volume fraction exponent.

REFERENCES

Arciniega RA, Reddy JN (2007). Large deformation analysis of functionally graded shells. Int. J. Solids Struct., 44: 2036-2052.

Bolotin VV (1964). The Dynamic Stability of Elastic Systems. Holden-Day, San Francisco, pp. 145-162.

Gong SW, Lam KY, Reddy JN (1999). The elastic response of functionally graded cylindrical shells to low-velocity impact. Int. J. Impact Eng., 22: 397-417.

Koizumi M, Niino M (1995). Overview of FGM research in Japan, MRS Bull., 20: 19-21.

Loy CT, Lam KY, Reddy JN (1999). Vibration of functionally graded cylindrical shells. Int. J. Mech. Sci., 41: 309-24.

Ng TY, Lam KM, Liew KM, Reddy JN (2001). Dynamic stability analysis of functionally graded cylindrical shells under periodic axial loading. Int. J. Solids Struct., 38: 1295-309.

Praveen GN, Chin CD, Reddy JN (1999). Thermoelastic Analysis of a Functionally Graded Ceramic-Metal Cylinder. ASCE J. Eng. Mech., 125(11): 1259-1267.

Pradhan SC, Loy CT, Lam KY, Reddy JN (2000). Vibration characteristics of functionally graded cylindrical shells under various boundary conditions. Applied Acoustics. 61: 119-29.

Reddy JN (2004). Mechanics of Laminated Composite Plates and Shells. Second Edition, CRC Press, New York, pp. 201-244.

Reddy JN, Chin CD (1998). Thermomechanical Analysis of Functionally Graded Cylinders and Plates. J. Thermal Stresses, 26(1): 593-626.

Sofiyev AH (2005). The stability of compositionally graded ceramic–metal cylindrical shells under a periodic axial impulsive loading. Comp. Struct., 69: 247-57.

APPENDIX A

$T_{11} = A_{11}\lambda_m^2 + \frac{A_{66}n^2}{R^2}$	$T_{12} = -\frac{A_{12} + A_{66}}{R}\lambda_m n$	$T_{13} = -\frac{A_{12}}{R}\lambda_m$
$T_{14} = B_{66}\lambda_m^2 + \frac{B_{66}n^2}{R^2}$	$T_{15} = -\frac{B_{12} + B_{66}}{R}\lambda_m n$	$T_{21} = -\frac{A_{12} + A_{66}}{R}\lambda_m n$
$T_{22} = A_{66}\lambda_m^2 + \frac{A_{22}n^2}{R^2} + \frac{C_{55}}{R^2}$	$T_{23} = \frac{A_{22} + C_{55}}{R}n$	$T_{24} = -\frac{B_{21} + B_{66}}{R}\lambda_m n$
$T_{25} = B_{66}\lambda_m^2 + \frac{B_{22}n^2}{R^2} - \frac{C_{55}}{R^2}$	$T_{31} = -\frac{A_{21}}{R}\lambda_m$	$T_{32} = \frac{C_{55} + A_{22}}{R^2}n$
$T_{33} = C_{44}\lambda_m^2 + \frac{C_{55}n^2}{R^2} + \frac{A_{22}}{R^2}$	$T_{34} = \left(C_{44} - \frac{B_{21}}{R}\right)\lambda_m$	$T_{35} = -\frac{C_{55}R - B_{22}}{R^2}n$
$T_{41} = B_{11}\lambda_m^2 + \frac{B_{66}n^2}{R^2}$	$T_{42} = -\frac{B_{12} + B_{66}}{R}\lambda_m n$	$T_{43} = \left(C_{44} - \frac{B_{12}}{R}\right)\lambda_m$
$T_{44} = D_{11}\lambda_m^2 + \frac{D_{66}n^2}{R^2} + C_{44}$	$T_{45} = -\frac{D_{12} + D_{66}}{R}\lambda_m n$	$T_{51} = -\frac{B_{21} + B_{66}}{R}\lambda_m n$
$T_{52} = B_{66}\lambda_m^2 + \frac{B_{22}n^2}{R^2} - \frac{C_{55}}{R}$	$T_{53} = \frac{B_{22} - RC_{55}}{R^2}n$	$T_{55} = \frac{D_{22}}{R^2}n^2 + C_{55} + \frac{D_{66}}{R}\lambda_m^2$
$T_{54} = -\frac{D_{21}}{R}\lambda_m n - \frac{D_{66}}{R}\lambda_m n$		